HHS Public Access

Author manuscript

Microbes Infect. Author manuscript; available in PMC 2015 November 01.

Published in final edited form as:

Microbes Infect. 2014 November ; 16(11): 923–935. doi:10.1016/j.micinf.2014.08.016.

Molecular imaging, biodistribution and efficacy of mesenchymal bone marrow cell therapy in a mouse model of Chagas disease

Jasmin[a,b], **Linda A Jelicks, PhD**[c], **Herbert B Tanowitz, MD**[d,e], **Vera Maria Peters, PhD**[f], **Rosalia Mendez-Otero, MD, PhD**[a], **Antonio C Campos de Carvalho, MD, PhD**[#a,b], and **David C Spray, PhD**[#b,d]

[a] Instituto de Biofísica Carlos Chagas Filho, Universidade Federal do Rio de Janeiro, RJ, Brazil

[b] Dept. of Neuroscience, Albert Einstein College of Medicine, NY, USA

[c] Dept. of Physiology and Biophysics, Albert Einstein College of Medicine, NY, USA

[d] Dept. of Pathology, Albert Einstein College of Medicine, NY, USA

[e] Dept. of Medicine, Albert Einstein College of Medicine, NY, USA

[f] Centro de Biologia da Reprodução, Universidade Federal de Juiz de Fora, MG, Brazil

[#] These authors contributed equally to this work.

Abstract

Chagasic cardiomyopathy, resulting from infection with the parasite *Trypanosoma cruzi*, was discovered more than a century ago and remains an incurable disease. Due to the unique properties of mesenchymal stem cells (MSC) we hypothesized that these cells could have therapeutic potential for chagasic cardiomyopathy. Recently, our group pioneered use of nanoparticle-labeled MSC to correlate migration with its effect in an acute Chagas disease model. We expanded our investigation into a chronic model and performed more comprehensive assays. Infected mice were treated with nanoparticle labeled MSC and their migration was correlated with alterations in heart morphology, metalloproteinase activity, and expression of several proteins. The vast majority of labeled MSC migrated to liver, lungs and spleen whereas a small number of cells migrated to chagasic hearts. Magnetic resonance imaging (MRI) demonstrated that MSC therapy reduced heart dilatation. Additionally metalloproteinase activity was higher in heart and other organs of infected mice. Protein expression analyses revealed that connexin 43, laminin γ1, IL-10 and INF-γ were affected by the disease and recovered after cell therapy. Interestingly, MSC therapy led to upregulation of SDF-1 and c-kit in the hearts. The beneficial effect of MSC therapy in Chagas disease is likely due to an indirect action of the cells of the heart, rather than the incorporation of large numbers of stem cells into working myocardium.

Corresponding Authors: David C Spray david.spray@einstein.yu.edu Phone Number: (1-718) 430-2537 Dept. Neuroscience, AECOM, 1410 Pelham Pkway, Bronx, NY 10461, USA; Antonio C Campos de Carvalho acarlos@biof.ufrj.br Phone Number: (55-21) 2562-6559 Av. Carlos Chagas Filho, 373, CCS - Bl.G, G2-028, UFRJ, Rio de Janeiro, RJ, Brazil, CEP: 21941-902.

Keywords

Chagas disease; cardiomyopathy; cellular therapy; mesenchymal stem cells; cells tracking

1. Introduction

The protozoan parasite that causes Chagas disease, *Trypanosoma cruzi*, is naturally transmitted by hematophagous triatomine insects and affects approximately 15–16 million people in Latin American countries [1]. It is a serious public health problem due to the impact on worker productivity, premature disability and death. The parasite can also be transmitted by blood transfusion, organ transplantation or congenitally [2, 3]. Thus, although originally limited to Latin America there is an increased concern about Chagas disease in the United States and Europe due to the large number of immigrants from endemic areas [3-6]. The acute phase of the disease is difficult to diagnose [7] and the clinical acute manifestations disappear in weeks to months. The disease then enters the chronic phase, generally starting with a long period of clinical latency called the indeterminate form. During the indeterminate form approximately 30% of infected individuals develop a symptomatic chronic phase, of which 10% display gastrointestinal diseases and 90% develop heart disease [8]; there is no consensus regarding the efficacy of anti-parasitic drugs benznidazole and nifurtimox during the chronic phase [9].

Chronic Chagas heart disease is a progressive, fibrotic inflammatory cardiomyopathy that results in irreversible heart damage [10] which leads to dilation and arrhythmias, and ultimately to congestive heart failure, the primary cause of death in these patients [11, 12]. As the disease progresses, few therapeutic options are left and they are identical to those for congestive heart failure of other etiologies and often include β-blockers, diuretics, angiotensin-enzyme inhibitors angiotensin receptor blockers and amiodarone. These treatments are often not satisfactory and the last therapeutic option is often heart transplantation [13]. In that complex scenario, cell therapy appears as an alternative for Chagas disease therapy.

Mesenchymal stem cells (MSC) are a rare subset of stem cells residing in the bone marrow where they closely interact with hematopoietic stem cells and support their growth and differentiation. MSC can differentiate into multiple mesenchymal cell types providing a promising tool for tissue repair [14]. In addition, MSC suppress many T cell, B cell and natural killer cell functions and may also affect dendritic cell activities. Therefore, given the established role of the immune system in the physiopathology of Chagas disease [15] and the immune modulatory properties of MSC we hypothesized that MSC could be an optimal cell type for therapy in chagasic cardiomyopathy.

In a previous study that we pioneered, we investigated the migration of transplanted MSC in an acute model of Chagas disease, and correlated MSC biodistribution with glucose metabolism and morphology of heart in chagasic mice by small animal positron emission tomography (microPET). It was observed that a small but significant number of transplanted labeled MSC migrated to chagasic hearts, whereas the vast majority of labeled MSC migrated to liver, lungs and spleen. Additionally, using the radioactive tracer [^{18}F] fluoro-2-

deoxyglucose, it was possible to demonstrate by microPET that therapy with MSC reduced right ventricular dilation and increased heart glucose metabolism [16].

In the present study, we extend our studies of MSC transplantation to a chronic murine model. Furthermore, we labeled the cells with two types of nanoparticles to correlate MSC migration with heart morphology and protein expression and global distribution of metalloproteinase activity.

2. Material and Methods

2.1. Mice

All experiments were initiated in 8-10 week old adult male mice CD-1 in accordance with the U.S. NIH Guide for the Care and Use of Laboratory Animals (NIH Publication No. 80-23), approved by the Institutional Animal Care and Use Committee of the Albert Einstein College of Medicine. The animal protocol numbers are 20130202 and 20110307.

2.2. Obtaining Mesenchymal Cells from Bone Marrow

Bone marrow cells were obtained from mouse tibias and femurs. The bones were isolated, epiphyses were removed and individually inserted in 1 mL automatic pipette tips inside 15 mL tubes. The bones were centrifuged at 300 × g for 1 min and the pellets suspended in Dulbecco's modified Eagle's high glucose medium (DMEM; Invitrogen Inc., Carlsbad,CA), supplemented with 10% fetal bovine serum (Invitrogen Inc.), 2 mM l-glutamine (Invitrogen Inc.), 100 U/mL penicillin (Sigma-Aldrich Co., St. Louis, MO), and 100 g/mL streptomycin (Sigma-Aldrich). The cells were plated in culture dishes with supplemented DMEM and maintained in 5% CO_2 atmosphere at 37°C. After 48-72 hrs of culture the medium was replaced to remove non adherent cells and the adherent cells were grown to confluence before each passage. Medium was replaced three times a week and all experiments were performed on second or third passage cells.

2.3. Mesenchymal Cell Labeling

Since each imaging modality has its inherent limitations, we used two different nanoparticle approaches to label and track MSC. Thus, the cells were labeled with magnetic and fluorescent nanoparticles which can be visualized by magnetic resonance imaging (MRI) and in vivo imaging system (IVIS), respectively.

2.3.1. Magnetic Nanoparticles—Feridex IV (Advanced Magnetics Inc., Cambridge) is a superparamagnetic iron oxide nanoparticle coated with dextran; it and another, dextran-coated ferumoxide, are clinically used as intravenous MRI contrast agents for analyzing liver pathology. Although dextran-coated SPION do not show sufficient cellular uptake by MSC, cationic compounds, such as protamine, facilitate the interaction with the negatively charged cell surface and subsequent enable endosomal uptake [17, 18]. Feridex was combined with Protamine chlorhydrate (Valeant Pharmaceuticals International, SP, Brazil) in culture medium and shaken for 30 minutes. The solution containing Feridex and protamine was added to MSC cultures at a proportion of 1:1 with supplemented DMEM in 5% CO_2 atmosphere at 37°C for 4 hours. The final concentration of protamine was 5 μg/mL

and of Feridex was 50 μg/mL. The labeled cells were washed three times with phosphate-buffered saline (PBS), trypsinized and transplanted in infected and not infected animals for MRI tracking.

2.3.2. Fluorescent Nanoparticles—For fluorescence tracking we used X-Sight761 nanospheres (Carestream Health Inc., Rochester, NY) which are fluorescent nanoparticles (17 nm in diameter) with a near infrared (NIR) wavelength 761 nm excitation and 789 nm emission. MSCs were incubated with a solution of 0.3 mg/mL X-Sight with supplemented DMEM in 5% CO_2 atmosphere at 37°C for 4 hours. For MSC X-Sight labeling an incorporation facilitator is not necessary [18]. The cells labeled with X-Sight were then washed with PBS, trypsinized and transplanted in chagasic and control animals for IVIS tracking. To define the basal autofluorescence we acquired images of control animals not-treated with cells and of chagasic animals treated with non-labeled cells.

Leakage of particles by exocytosis or cell death can provide misleading information regarding tissue distribution. Therefore, to determine the pattern of free nanoparticle distribution and compare with the distribution pattern of labeled cells, we performed injections of free X-Sight761, by tail vein, in control and chagasic mice 2 months after infection (2MAI) (0.5 mg/mL X-Sight in 100 μL PBS, as recommended by manufacturer).

2.4. *Trypanosoma cruzi* Infection and Therapy

The Brazil strain of *T. cruzi* was maintained in our laboratory by serial passage in C3H strain mice. CD-1 strain mice were infected by intraperitoneal injection of 5×10^4 trypomastigotes in saline solution. PBS alone (100 uL) or 3×10^6 MSC in PBS (~7.5×10^7 cells/kg) were transplanted in a single dose in control or chagasic mice 2MAI via tail vein.

The exact time-point separating the acute and chronic phases of Chagas disease in the murine model is not well defined. However, because the majority of the animals died 45 days after infection we considered mice that survived this as chronic chagasic animals.

2.5. Magnetic Resonance Imaging of Heart

For labeled MSC visualization and morphological analysis of hearts by MRI, mice were anesthetized with isoflurane inhalation anesthesia (2-3% in medical air) administered via a nose cone. A set of Gould ECG leads with thin silver wire contacts were attached under the skin to the four limbs and the ECG signal was fed to a Gould ECG amplifier linked to the MRI system and to a PC running Ponemah Physiology software. Heart rate and ECG were monitored continuously and used as the gating signal triggering the MRI spectrometer acquisition a Omega 9.4-T vertical bore MR system (Fremont, CA)) equipped with an S50 shielded gradient microimaging accessory and a 40 mm inner diameter-60 mm long 1H quadrature birdcage imaging coil (RF Sensors, LLC; NYC, NY). The spectrometer gating delay was set to acquire data during diastole using the R-wave of the ECG as the trigger signal. Several multislice spin-echo imaging data sets with an echo time of 18 ms and a repetition time of approximately 200-300 ms were acquired. A 51-mm field of view with a 128×256 matrix size (interpolated to 256×256) was used. In each mouse the image representing the midpoint between the base and apex of the heart was chosen for comparison

of the RV wall thickness and inner chamber diameter. MRI data were processed off-line with MATLAB-based MRI analysis software.

Images of control animals were acquired at a single time point (2 months). Images from infected animals were acquired before treatment or 24 hours, 1 week, 2 weeks, 1 and 2 month after transplantation. For all groups n=6, with exception of 2MAI (n=12).

2.6. Tracking X-Sight 761-Labeled Mesenchymal Cells

The X-Sight761 was visualized by IVIS Kodak Image Station 4000MM PRO (Carestream Health) equipped with a CCD camera. The machine was configured for 760 nm excitation, 830 nm emission, 3 min exposure, 2 × 2 binning and f-stop 2.5. The acquired images were analyzed with the Carestream MI Application 5.0.2.30 software (Carestream Health).

Whole body images were acquired from the ventral surface of the mice. Due to limited penetration depth and poor spatial resolution, we isolated organs of interest, including heart, bladder, lung, liver, spleen and kidney to perform ex vivo imaging. The images were acquired 2 or 15 days after labeled cell transplantation (MSC761 2d or MSC761 15d) or free nanoparticle injection (only761 2d and only761 15d) and images of age matched control animals were acquired for each time point. In Figure 2, the sample number was 3-4, and in Figure 3 it was 4-5 in each group (the same number of organs exposed in those figures).

2.7. Cell Visualization by Confocal Microscopy

The hearts were fixed overnight in 4% paraformaldehyde and sliced in 5 m frozen sections. The photomicrographs shown in this study were obtained using a Zeiss LSM 510 Duo confocal microscope.

2.8. Distribution of Metalloproteinase

We were the first researchers to use a fluorescent probe to detect matrix metalloproteinase (MMP) by IVIS technique in Chagas disease. The MMPSense 750 FAST (PerkinElmer, Inc., Boston, MA) is a MMP activatable agent that is optically silent upon injection but produces fluorescent signal (761 nm excitation and 789 nm emission) after cleavage by MMP-2, -3, -7, -9, -12 and -13. Control or chagasic animals treated with PBS or MSC received by tail vein a dose of 2 nM MMPSense in 100 μL of PBS one month after therapy (the sample number was 4-6 in each group, the same number of organs exposed in Figure 5). After 48 hours the images from ventral surface and ex vivo tissues (heart, bladder, lung, liver, spleen, kidney, leg muscle, brown and white fat) were acquired using the IVIS Kodak Image Station configured as described in item 2.6.

2.9. Protein Expression in the Hearts

The hearts were lysed in lysis buffer supplemented with protease inhibitor cocktail (Roche Laboratories, Basel, Switzerland) and protein concentration was determined by BCA protein assay kit (Pierce, Rockford, IL). The extracted protein was electrophoresed on 10% sodium dodecyl sulfate-polyacrylamide gel electrophoresis (Bio-Rad, Hercules, CA) and proteins were transferred onto nitrocellulose membranes (Whatman Int., Dassel, Germany). After 30-min incubation with 2% nonfat dry milk in tris buffer saline (TBS) containing 0.05%

Tween-20 (Sigma-Aldrich), the membranes were incubated overnight with the primary antibody or mouse GAPDH 36kDa (1:25,000; Fitzgerald Ind. Int., Acton, MA) at 4°C. Following three washes in TBS-Tween-20, the membranes were incubated with secondary antibodies goat anti-mouse or anti-rabbit IgG (1:10,000; Santa Cruz) for 1 h at room temperature. Detection of bands was performed after incubation with chemiluminescence reagents (Amersham Pharmacia Biotechnology, Piscataway, NJ). The sample number was 4-6 in each group.

The proteins were analyzed in control (age matched for each time point), chagasic mice 2MAI and chagasic mice 1 and 2 months after therapy, with the exception of c-kit and iNOS, which were analyzed only 2 months after therapy. The analyzed proteins were: interleukin (IL)-10; IL-1β; interferon (INF)-γ; connexin 43 (cx43); connexin 37 (Cx37); occludin; laminin γ-1; cleaved MMP-2; endothelin-1 (ET-1); stromal cell-derived factor-1 (SDF-1); signal transducer and activator of trascription 1 (Stat1); c-Kit; inducible nitric oxide synthase (iNOS); cardiac troponin T (cTnT); dystrophin and caveolin 3. Densitometric analysis of the western blots was performed using Image J software (http://rsb.info.nih.gov/ij/).

2.10. Statistical Analysis

The statistical significance was evaluated by non-parametric Kruskal-Wallis test with Dunns post-test using GraphPad Prism 5 (GraphPad Software, San Diego, CA) and $p<0.05$ was considered as statistically significant. The data are presented as mean and the error bars represent the standard error of the mean.

3. Results

3.1. In Vivo Magnetic Resonance Imaging

By MRI we analyzed heart morphology and visualized Feridex-labeled cells in the heart. We observed a significant dilation in right ventricle (RV) 2MAI when compared to control group (Figure 1) that was most apparent 3 months post-infection (2MAI+PBS 1M). However, cell therapy resulted in a significant reduction of the RV diameter 2 months after transplantation, showing similar values to the control group. No significant reduction was observed before 2 months post cell transplantation despite the high tendency observed 1 month after cellular therapy. No difference in heart rate was observed.

We were not able to detect Feridex-labeled cells in the cardiac images obtained by our MRI at 24 hours, 1 week, 2 weeks, 1 and 2 months after therapy.

3.2. Cell Detection by In Vivo Imaging System

As demonstrated in our previous study, the MSC efficiently incorporate X-Sight nanoparticles into the cell cytoplasm, without effects on proliferation or viability [18]. Since cells can release the nanoparticles generating nonspecific signals, injection of Sight761 nanoparticles was performed in control and chagasic mice to determine its distribution pattern and to compare with the pattern of X-Sight-labeled cells. We observed a high fluorescence signal in the body and organs at 2 days after free X-Sight761 injection (Figure

2). Of note, a higher concentration of free X-Sight761, approximately 60% of total fluorescence, was observed in the liver 2 days post-injection. From 2 days to 15 days post-injection a decrease of approximately 40% in total intensity was observed when we accounted for fluorescence signals in all organs, indicating that free nanoparticles are rapidly eliminated. Furthermore we could not see differences in free nanoparticle distribution between non-infected and infected animals, with the exception of the kidneys, where only the non-infected animals showed significantly higher fluorescence than the control (not injected with nanoparticle) group. Comparing the percentages of free nanoparticle distribution and elimination with the groups treated with X-Sight-labeled MSC we observed that in the labeled cells approximately 80% of the fluorescence analyzed was localized in the liver and the mean intensity decreased approximately 60% from 2 to 15 days post-injection, revealing a different distribution pattern (Figure 3) thus indicating that the pattern observed with the labeled cells is not the result of cell death and free nanoparticle distribution.

Analysis of cell distribution in infected and non-infected animals reveals interesting patterns. First and foremost, there is no significant difference in fluorescence in the heart between the infected and non-infected groups. This indicates that the chronic infection does not promote a significant homing of the MSC to the heart. Overall, we could not detect differences in fluorescence in any of the ex-vivo examined organs between the MSC-injected infected and non-infected animals. The biodistribution of the MSC revealed that lungs, liver and spleen were the organs that concentrated the majority of the injected cells, 2 days post-injection, in both infected and non-infected animals. Of note, the bladder and the kidneys did not show increased fluorescence 2 days after cell injection. Furthermore, fluorescence in the bladder was higher in both infected and non-infected animals 15 days post-injection, suggesting urinary elimination of cells or more probably of free nanoparticles.

Confocal microscopy detected a few fluorescent cells in the hearts of chagasic mice treated with X-Sight-labeled MSC (Figure 4). In control mice not treated with labeled cells fluorescence was not detectable (Figure 4A). In non-infected mice treated with labeled cells some red spots could be detected as shown in Figure 4B. But infected animals exhibited a higher fluorescence than non-infected ones (compare 4B and C).Given the differences in sensitivity of the two methods (*in vivo* imaging versus microscopic imaging) and the trend shown in Figure 3C our results suggest that, at the most, MSC may have a slight cardiac tropism in the chagasic mice.

All analyzed organs were weighed and found to be unaffected by the infection, except the spleen. The spleens of the chagasic animals were heavier than control (93.2±7.3; 165.6±5.2 and 174.5±19.9 mg, for control or chagasic mice treated with PBS or MSC, respectively). In addition we performed body composition analysis by magnetic nuclear resonance (Echo MRI 2004; Bruker Corporation, Billerica, MA) to measure the percentage of water, fat and lean in vivo and no differences were observed among the groups (data not shown).

3.3. Distribution of Metalloproteinase

Using MMPSense750 it was possible to detect MMP in several regions of the mice (Figure 5A-G). In ventral surface images a higher fluorescence intensity, due to MMP presence, was

observed in chagasic groups than in controls (Figure 5A-B). In heart and white fat we observed a higher signal in MSC treated animals when compared to controls (Figure 5D and F), and in spleen and leg muscle we observed a higher signal in PBS treated animals (Figure E and G). However, there was no difference in MMP activity between PBS or MSC treated chagasic animals, suggesting that increased metalloproteinase activity in these organs is due to the infection alone. Other analyzed organs, such as bladder, lung, liver, kidney and brown fat did not present differences in MMP expression, as can be observed in Figure 5C.

We performed western blots to analyze cleaved MMP-2 in heart samples, and we observed a significantly higher expression of MMP-2 in all chagasic mice independent of PBS or MSC treatment. We observed that MMP-2 expression significantly decreased after 4 months post-infection, when compared with 3 months, despite still being statistically different from the control group (Figure 5H).

3.4. Protein Expression in the Heart

Expression of specific proteins in the heart was evaluated before, 1 and 2 months after cell therapy to evaluate long-term effects of MSC transplantation. Among others, gap and tight junction, extracellular matrix and inflammatory proteins were analyzed.

We analyzed the gap junction proteins Cx43 and Cx37, and the tight junction protein occludin. Cx43 (the major cardiac connexin) showed lower expression 2 months after infection when compared to control, a tendency in all chagasic animals treated with PBS. However, after 2 months of MSC therapy in chagasic mice, the Cx43 expression level was higher than in the PBS treated group (Figure 6A). No alteration in Cx37 (the major connexin expressed in endothelial cells of heart) expression was observed among the groups. Occludin, an important component of tight junctions, was upregulated by Chagas disease in both PBS and MSC groups (Supplemental Figure).

The extracellular matrix protein laminin γ1 showed upregulation in hearts of infected animals 4 months after infection (2MAI+PBS 2M) when compared to control, but this was not observed in the cell treated group (Figure 6B).

We investigated the expression of relevant proinflammatory (IL-1β, SDF-1and INF-γ) and anti-inflammatory (IL-10) cytokines in heart samples. Expression of IL-1β increased in all infected mice at all time-points (Supplemental Figure). The expression of INF-γ and IL-10 was increased in all chagasic mice with the exception of those treated with MSC for 2 months (Figure 6C and D, respectively). In Figure 6E, it is important to note that SDF-1 expression was upregulated only by MSC therapy. These data suggest that MSC therapy not only has an immunomodulatory effect in the heart of infected mice, but also promotes the migration of stem/progenitor cells to the heart by up-regulating the SDF-1 axis.

The c-Kit protein, a transmembrane receptor responsible for chemotaxis, proliferation, apoptosis and cell adhesion was analyzed 2 months after therapy. It showed a higher expression in chagasic mice treated with MSC when compared to the control group (Figure 6F). Representative images of western blots for all proteins analyzed are shown in Figure 6G.

We also analyzed other proteins with diverse functions in the heart, such as ET-1 (vasoconstrictor), Stat1 (mediates cellular response to interferons, cytokine, and other cytokines and growth factors), iNOS (responsible for nitric oxide production in cardiovascular system), cTnT (important in the regulation of cardiac contraction), dystrophin (connect muscle fiber cytoskeleton with the extracellular matrix) and caveolin 3 (may act as scaffolding proteins within caveolar membranes by compartmentalizing and concentrating signaling molecules). We observed that ET-1, Stat1 and iNOS were upregulated as a result of infection in PBS or MSC treatment. Regarding cTnT, dystrophin and caveolin 3, no alterations were observed (Supplemental Figure).

4. Discussion

Recently, our group described the biodistribution and effect of MSC therapy in acute *T. cruzi* infection [16]. We have now extended studies of cell therapy in this incurable disease by treating chronically infected mice with MSC. In addition to our previous study with MSC, only two types of cell therapy approaches have been applied to animal models of Chagas disease: Bone marrow mononuclear cells in mice [19-21] and co-cultured skeletal myoblasts with MSC in rats [22]. In addition, bone marrow mononuclear cells were transplanted in patients with end-stage heart failure due to Chagas disease but significant improvement in cardiac function was not observed [23]. It has been suggested that MSC is a more appropriate cell type for cardiac cell therapy than other cell types, such as skeletal myoblasts, due to their capacity to electrically couple to host cardiac myocytes [24] which does not occur with skeletal myoblasts [25].

Although our Chagas mouse model has several similarities with the human form of the disease, we did not observe functional abnormalities in the left ventricle (LV) by echocardiogram (data not shown) and MRI up to 3 months after infection. However other studies from our group using the same mouse and parasite strains did report left ventricular dysfunction 150 [26] and 200 days post-infection [27]. In addition our group has considered right ventricular (RV) remodeling as a hallmark of chagasic heart disease in the murine model [18, 21, 28-30] because the RV diameter increases in the acute phase and this persists into the chronic phase [18, 29]. Validating these observations in these mouse studies, it was demonstrated that RV dysfunction can be used to predict mortality in chagasic patients [31]. Here we observed RV dilation in chagasic animals and after MSC therapy reduction of the ventricular dimensions to control levels after MSC therapy, but we were not able to visualize Feridex-labeled cells in the heart. Our inability to detect intravenously transplanted MSC in the heart is consistent with other reports[32]. However, cells can be detected following intracoronary or intramuscular injection [33-35]. We previously showed that Feridex-labeled MSC can be visualized after direct injection into leg muscle [16, 17] or into striatum [36].

In accordance with not being able to detect the tail vein injected cells by MRI, it was also not possible to detect cells labeled with the fluorescent nanoparticle through IVIS. The majority of X-Sight-labeled MSC migrated to liver, lung and spleen, which is consistent with studies in the canine model of infarction [32] and in patients with cirrhosis [37]. Close inspection of cell migration by confocal microscopy revealed a higher migration of labeled MSC to chagasic hearts 2 days after injection. The preferential migration of MSC to the

injured tissue has been reported in other models, such arthritic joints [38] and stroke [39]. Of note, in chagasic patients treated with intracoronary injection of mononuclear cells labeled with technetium 99m a very low intensity of radioactivity was found in the hearts compared with other organs such as liver and spleen [40].

The fluorescence intensity 15 days after transplantation was greatly reduced, which is likely due to nanoparticle exocytosis, cellular proliferation and/or cell death. Based on the possibility that nanoparticles might be released and secondarily label other cells, such as macrophages, we injected free X-Sight in the mice to compare the distribution pattern. In contrast to the distribution of labeled cells, free X-Sight was distributed more widely in whole body. In addition, in the heart there was no difference in the intensity of free nanoparticles between chagasic and control. Thus, the distribution of free nanoparticles was different from that of labeled cells, and we believe that the majority of observed fluorescence 2 days after therapy reflects cell distribution and not that of released nanoparticles.

The exact mechanisms and molecules involved in MSC migration to injured areas are unknown. It is assumed that the MSC migration process is similar to that of leukocytes, where various molecules are involved, including chemokines and their receptors, adhesion molecules and proteases [41]. The extracellular matrix degradation by enzymes, such as the MMP, allows migration of leukocytes [41] attracted by the cytokine gradient in the injured tissue. Here we found, using western blot to cleaved MMP-2, that its expression was upregulated in chagasic heart, implying that MSC migration to infected heart could be facilitated, in part, by MMP-2. Although MMPs are essential for migration process of inflammatory cells, their uncontrolled activity contributes to chronic inflammation and tissue damage. In addition, it has been shown that MMP-2 and MMP-9 can cleave and modulate the activity of several cytokines [42, 43]. Recently, the presence of MMP-9-like molecules in *T. cruzi* has been reported, which could possibly promote parasite dissemination [44]. Here, we applied a novel method to analyze the expression of MMP in chagasic animals using a fluorescent probe, with which we observed that not only the heart but other tissues were affected by the infection, including spleen, leg muscle and white fat. The MMPSense750 technique is less sensitive to detect these proteins than western blotting; however, it is a very useful method to obtain a global visualization of MMP activity.

The migration process of MSC can be induced by various proteins such as SDF-1, platelet-derived growth factor, insulin-like growth factor 1 and IL-6 [45]. It has been suggested that IL-1β can activate adherence properties in MSC [46]. The migration of hematopoietic [47] and cardiac stem cells [48] has been related to SDF-1 expression as well. In the present study we observed that SDF-1 was upregulated by MSC treatment, which supports the premise that these cells release factors, in a paracrine mode, thereby recruiting circulating stem cells and tissue stem cells. In addition SDF-1 can induce proliferation, adhesion and secretion of MMP and angiogenic factors [49].

T. cruzi infection modulates the production of several cytokines by macrophages, T and B cells and in a small number of natural killer cells [15]. Here we analyzed the cytokines IL-1β, IL-10 and INF-γ, and observed that each was upregulated by the disease. However,

after 2 months of MSC therapy, reduction of IL-10 and INF-γ expression was notable, indicating the immunomodulatory effect of MSC. It is important to emphasize that most MSC die within days or weeks of transplantation, yet their beneficial effects can be seen over a much longer term, suggesting a critical time window for MSC action [50].

As in other arrhythmogenic heart diseases, chagasic cardiomyopathy is associated with a decrease in expression of the gap junction protein Cx43 [51]. Consistent with previous studies [51], we observed the downregulation of Cx43 in chagasic animals which was reestablished by MSC treatment. Although we did not observe arrhythmias in our model, the altered expression is itself a very interesting result. In addition, MSC therapy slightly reversed the upregulation of laminin γ1 observed in chagasic animals indicating a reduction in extracellular matrix that is also important to reduce possible arrhythmias. We also analyzed c-kit, which was upregulated by MSC treatment while showing just a tendency to increase in PBS treated chagasic animals. It has been reported that c-kit is expressed in cardiac and hematopoietic stem cells, thus, it is possible that *T. cruzi* infection results in the attraction of these cells to the injured tissue, but importantly MSC therapy significantly increases c-kit in the heart. An increase in the number of cardiac stem cells in the heart of a myocardial infarction model has also been reported [52]. Taken together, the upregulation of c-kit and SDF-1 by MSC suggests that MSC can attract more stem cells to the injured tissue, which is likely important for tissue regeneration. Other upregulated proteins resulting from infection were ET-1, Stat-1 and iNOS but MSC treatment did not restore those proteins to control levels.

To summarize, in the present study we have extended our investigations of MSC therapy to the chronic stage of murine Chagas disease, demonstrating a beneficial effect of the cell therapy in restoring heart morphology and protein expression. Our observations suggest that the homing of the cells to heart is limited. Further, the similar biodistribution of the cells in the non-infected and infected animals, with a predominance of cell migration to lungs, liver and spleen, suggests that the benefits of this cell therapy are the result of systemic actions rather than to the incorporation of the cells into working myocardium.

Supplementary Material

Refer to Web version on PubMed Central for supplementary material.

Acknowledgments

We gratefully acknowledge Dazhi Zhao and Marcia Urban-Maldonado for technical assistance during the elaboration of this work. This work was supported by grants from the Conselho Nacional de Desenvolvimento Científico e Tecnológico (CNPq - Brazil) and National Institutes of Health: Fogarty training grant (D43-TW007129) and RO1 (HL73732).

References

1. Tanowitz HB, Machado FS, Jelicks LA, Shirani J, de Carvalho AC, Spray DC, et al. Perspectives on Trypanosoma cruzi-induced heart disease (Chagas disease). Prog Cardiovasc Dis. 2009; 51:524–539. [PubMed: 19410685]

2. Riera C, Guarro A, Kassab HE, Jorba JM, Castro M, Angrill R, et al. Congenital transmission of Trypanosoma cruzi in Europe (Spain): a case report. Am J Trop Med Hyg. 2006; 75:1078–1081. [PubMed: 17172369]

3. Otani MM, Vinelli E, Kirchhoff LV, del Pozo A, Sands A, Vercauteren G, et al. WHO comparative evaluation of serologic assays for Chagas disease. Transfusion. 2009; 49:1076–1082. [PubMed: 19290995]

4. Tarleton RL, Reithinger R, Urbina JA, Kitron U, Gurtler RE. The challenges of Chagas Disease--grim outlook or glimmer of hope. PLoS Med. 2007; 4:e332. [PubMed: 18162039]

5. Gascon J, Bern C, Pinazo MJ. Chagas disease in Spain, the United States and other non-endemic countries. Acta Trop. 2010; 115:22–27. [PubMed: 19646412]

6. Tanowitz HB, Weiss LM, Montgomery SP. Chagas disease has now gone global. PLoS Negl Trop Dis. 2011; 5:e1136. [PubMed: 21572510]

7. Miles MA, Feliciangeli MD, de Arias AR. American trypanosomiasis (Chagas' disease) and the role of molecular epidemiology in guiding control strategies. Bmj. 2003; 326:1444–1448. [PubMed: 12829559]

8. Munoz-Saravia SG, Haberland A, Wallukat G, Schimke I. Chronic Chagas' heart disease: a disease on its way to becoming a worldwide health problem: epidemiology, etiopathology, treatment, pathogenesis and laboratory medicine. Heart Fail Rev. 2010; 17:45–64. [PubMed: 21165698]

9. Clayton J. Chagas disease 101. Nature. 2010; 465:S4–5. [PubMed: 20571553]

10. Bonney KM, Engman DM. Chagas heart disease pathogenesis: one mechanism or many? Curr Mol Med. 2008; 8:510–518. [PubMed: 18781958]

11. Machado FS, Jelicks LA, Kirchhoff LV, Shirani J, Nagajyothi F, Mukherjee S, et al. Chagas heart disease: report on recent developments. Cardiol Rev. 2012; 20:53–65. [PubMed: 22293860]

12. Tanowitz HB, Kirchhoff LV, Simon D, Morris SA, Weiss LM, Wittner M. Chagas' disease. Clin Microbiol Rev. 1992; 5:400–419. [PubMed: 1423218]

13. Campos de Carvalho AC, Goldenberg RC, Jelicks LA, Soares MB, Dos Santos RR, Spray DC. Cell therapy in Chagas disease. Interdiscip Perspect Infect Dis. 2009; 2009:4843–58.

14. Bernardo ME, Pagliara D, Locatelli F. Mesenchymal stromal cell therapy: a revolution in Regenerative Medicine? Bone Marrow Transplant. 2012; 47:164–171. [PubMed: 21478914]

15. Cunha-Neto E, Nogueira LG, Teixeira PC, Ramasawmy R, Drigo SA, Goldberg AC, et al. Immunological and non-immunological effects of cytokines and chemokines in the pathogenesis of chronic Chagas disease cardiomyopathy. Mem Inst Oswaldo Cruz. 2009; 104(Suppl 1):252–258. [PubMed: 19753481]

16. Jasmin, Jelicks LA.; Koba, W.; Tanowitz, HB.; Mendez-Otero, R.; Campos de Carvalho, AC., et al. Mesenchymal bone marrow cell therapy in a mouse model of chagas disease. Where do the cells go? PLoS Negl Trop Dis. 2012; 6:e1971. [PubMed: 23272265]

17. Jasmin, Torres AL.; Nunes, H.; Passipieri, J.; Jelicks, L.; Gasparetto, E., et al. Optimized labeling of bone marrow mesenchymal cells with superparamagnetic iron oxide nanoparticles and in vivo visualization by magnetic resonance imaging. Journal of nanobiotechnology. 2011; 9:4. [PubMed: 21542946]

18. Jasmin, Torres AL.; Jelicks, L.; de Carvalho, AC.; Spray, DC.; Mendez-Otero, R. Labeling stem cells with superparamagnetic iron oxide nanoparticles: analysis of the labeling efficacy by microscopy and magnetic resonance imaging. Methods Mol Biol. 2012; 906:239–252. [PubMed: 22791437]

19. Soares MB, Lima RS, Rocha LL, Takyia CM, Pontes-de-Carvalho L, de Carvalho AC, et al. Transplanted bone marrow cells repair heart tissue and reduce myocarditis in chronic chagasic mice. Am J Pathol. 2004; 164:441–447. [PubMed: 14742250]

20. Soares MB, Lima RS, Souza BS, Vasconcelos JF, Rocha LL, Dos Santos RR, et al. Reversion of gene expression alterations in hearts of mice with chronic chagasic cardiomyopathy after transplantation of bone marrow cells. Cell Cycle. 2011; 10:1448–1455. [PubMed: 21467843]

21. Goldenberg RC, Jelicks LA, Fortes FS, Weiss LM, Rocha LL, Zhao D, et al. Bone marrow cell therapy ameliorates and reverses chagasic cardiomyopathy in a mouse model. J Infect Dis. 2008; 197:544–547. [PubMed: 18237267]

22. Guarita-Souza LC, Carvalho KA, Woitowicz V, Rebelatto C, Senegaglia A, Hansen P, et al. Simultaneous autologous transplantation of cocultured mesenchymal stem cells and skeletal myoblasts improves ventricular function in a murine model of Chagas disease. Circulation. 2006; 114:I120–124. [PubMed: 16820560]

23. Ribeiro Dos Santos R, Rassi S, Feitosa G, Grecco OT, Rassi A Jr. da Cunha AB, et al. Cell therapy in Chagas cardiomyopathy (Chagas Arm of the MiHeart Study): a multicenter randomized trial. Circulation. 2012; 125:2454–61. [PubMed: 22523306]

24. Boyle AJ, McNiece IK, Hare JM. Mesenchymal stem cell therapy for cardiac repair. Methods Mol Biol. 2010; 660:65–84. [PubMed: 20680813]

25. Reinecke H, MacDonald GH, Hauschka SD, Murry CE. Electromechanical coupling between skeletal and cardiac muscle. Implications for infarct repair. J Cell Biol. 2000; 149:731–740. [PubMed: 10791985]

26. Chen G, Barr S, Walsh D, Rohde S, Brewer A, Bilezikian JP. Cardioprotective actions of verapamil on the beta-adrenergic receptor complex in acute canine Chagas' disease. J Mol Cell Cardiol. 1996; 28:931–41. [PubMed: 8762032]

27. Jelicks LA, Chandra M, Shirani J, Shtutin V, Tang B, Christ GJ, et al. Cardioprotective effects of phosphoramidon on myocardial structure and function in murine Chagas' disease. Int J Parasitol. 2002; 32:1497–506. [PubMed: 12392915]

28. Huang H, Chan J, Wittner M, Jelicks LA, Morris SA, Factor SM, et al. Expression of cardiac cytokines and inducible form of nitric oxide synthase (NOS2) in Trypanosoma cruzi-infected mice. J Mol Cell Cardiol. 1999; 31:75–88. [PubMed: 10072717]

29. de Souza AP, Tang B, Tanowitz HB, Araujo-Jorge TC, Jelicks EL. Magnetic resonance imaging in experimental Chagas disease: a brief review of the utility of the method for monitoring right ventricular chamber dilatation. Parasitol Res. 2005; 97:87–90. [PubMed: 15986245]

30. Prado CM, Fine EJ, Koba W, Zhao D, Rossi MA, Tanowitz HB, et al. Micro-positron emission tomography in the evaluation of Trypanosoma cruzi-induced heart disease: Comparison with other modalities. Am J Trop Med Hyg. 2009; 81:900–905. [PubMed: 19861629]

31. Nunes Mdo C, Rocha MO, Ribeiro AL, Colosimo EA, Rezende RA, Carmo GA, et al. Right ventricular dysfunction is an independent predictor of survival in patients with dilated chronic Chagas' cardiomyopathy. Int J Cardiol. 2008; 127:372–379. [PubMed: 17689706]

32. Kraitchman DL, Tatsumi M, Gilson WD, Ishimori T, Kedziorek D, Walczak P, et al. Dynamic imaging of allogeneic mesenchymal stem cells trafficking to myocardial infarction. Circulation. 2005; 112:1451–1461. [PubMed: 16129797]

33. Hill JM, Dick AJ, Raman VK, Thompson RB, Yu ZX, Hinds KA, et al. Serial cardiac magnetic resonance imaging of injected mesenchymal stem cells. Circulation. 2003; 108:1009–1014. [PubMed: 12912822]

34. Graham JJ, Foltz WD, Vaags AK, Ward MR, Yang Y, Connelly KA, et al. Long-term tracking of bone marrow progenitor cells following intracoronary injection post-myocardial infarction in swine using MRI. Am J Physiol Heart Circ Physiol. 2010; 299:H125–133. [PubMed: 20418483]

35. Amsalem Y, Mardor Y, Feinberg MS, Landa N, Miller L, Daniels D, et al. Iron-oxide labeling and outcome of transplanted mesenchymal stem cells in the infarcted myocardium. Circulation. 2007; 116:I38–45. [PubMed: 17846324]

36. Moraes L, Vasconcelos-dos-Santos A, Santana FC, Godoy MA, Rosado-de-Castro PH, Jasmin, et al. Neuroprotective effects and magnetic resonance imaging of mesenchymal stem cells labeled with SPION in a rat model of Huntington's disease. Stem Cell Res. 2012; 9:143–155. [PubMed: 22742973]

37. Gholamrezanezhad A, Mirpour S, Bagheri M, Mohamadnejad M, Alimoghaddam K, Abdolahzadeh L, et al. In vivo tracking of 111In-oxine labeled mesenchymal stem cells following infusion in patients with advanced cirrhosis. Nucl Med Biol. 2011; 38:961–967. [PubMed: 21810549]

38. Sutton EJ, Henning TD, Boddington S, Demos S, Krug C, Meier R, et al. In vivo magnetic resonance imaging and optical imaging comparison of viable and nonviable mesenchymal stem cells with a bifunctional label. Mol Imaging. 2010; 9:278–290. [PubMed: 20868628]

39. Jang KS, Lee KS, Yang SH, Jeun SS. In vivo tracking of transplanted bone marrow-derived mesenchymal stem cells in a murine model of stroke by bioluminescence imaging. J Korean Neurosurg Soc. 2010; 48:391–398. [PubMed: 21286474]
40. Barbosa da Fonseca LM, Xavier SS, Rosado de Castro PH, Lima RS, Gutfilen B, Goldenberg RC, et al. Biodistribution of bone marrow mononuclear cells in chronic chagasic cardiomyopathy after intracoronary injection. Int J Cardiol. 2011; 149:310–314. [PubMed: 20199816]
41. De Becker A, Van Hummelen P, Bakkus M, Vande Broek I, De Wever J, De Waele M, et al. Migration of culture-expanded human mesenchymal stem cells through bone marrow endothelium is regulated by matrix metalloproteinase-2 and tissue inhibitor of metalloproteinase-3. Haematologica. 2007; 92:440–449. [PubMed: 17488654]
42. McQuibban GA, Gong JH, Tam EM, McCulloch CA, Clark-Lewis I, Overall CM. Inflammation dampened by gelatinase A cleavage of monocyte chemoattractant protein-3. Science. 2000; 289:1202–1206. [PubMed: 10947989]
43. Opdenakker G, Van den Steen PE, Van Damme J. Gelatinase B: a tuner and amplifier of immune functions. Trends Immunol. 2001; 22:571–579. [PubMed: 11574282]
44. Nogueira de Melo AC, de Souza EP, Elias CG, dos Santos AL, Branquinha MH, d'Avila-Levy CM, et al. Detection of matrix metallopeptidase-9-like proteins in Trypanosoma cruzi. Exp Parasitol. 2010; 125:256–263. [PubMed: 20138866]
45. Tondreau T, Meuleman N, Stamatopoulos B, De Bruyn C, Delforge A, Dejeneffe M, et al. In vitro study of matrix metalloproteinase/tissue inhibitor of metalloproteinase production by mesenchymal stromal cells in response to inflammatory cytokines: the role of their migration in injured tissues. Cytotherapy. 2009; 11:559–569. [PubMed: 19551542]
46. Segers VF, Van Riet I, Andries LJ, Lemmens K, Demolder MJ, De Becker AJ, et al. Mesenchymal stem cell adhesion to cardiac microvascular endothelium: activators and mechanisms. Am J Physiol Heart Circ Physiol. 2006; 290:H1370–1377. [PubMed: 16243916]
47. Sharma M, Afrin F, Satija N, Tripathi RP, Gangenahalli GU. Stromal-derived factor-1/CXCR4 signaling: indispensable role in homing and engraftment of hematopoietic stem cells in bone marrow. Stem Cells Dev. 2011; 20:933–946. [PubMed: 21186999]
48. Tang JM, Wang JN, Zhang L, Zheng F, Yang JY, Kong X, et al. VEGF/SDF-1 promotes cardiac stem cell mobilization and myocardial repair in the infarcted heart. Cardiovasc Res. 2011; 91:402–411. [PubMed: 21345805]
49. Kucia M, Jankowski K, Reca R, Wysoczynski M, Bandura L, Allendorf DJ, et al. CXCR4-SDF-1 signalling, locomotion, chemotaxis and adhesion. J Mol Histol. 2004; 35:233–245. [PubMed: 15339043]
50. Laflamme MA, Murry CE. Heart regeneration. Nature. 2011; 473:326–335. [PubMed: 21593865]
51. Adesse D, Goldenberg RC, Fortes FS, Jasmin, Iacobas DA, Iacobas S, et al. Gap junctions and chagas disease. Adv Parasitol. 2011; 76:63–81. [PubMed: 21884887]
52. Urbanek K, Torella D, Sheikh F, De Angelis A, Nurzynska D, Silvestri F, et al. Myocardial regeneration by activation of multipotent cardiac stem cells in ischemic heart failure. Proc Natl Acad Sci U S A. 2005; 102:8692–8697. [PubMed: 15932947]

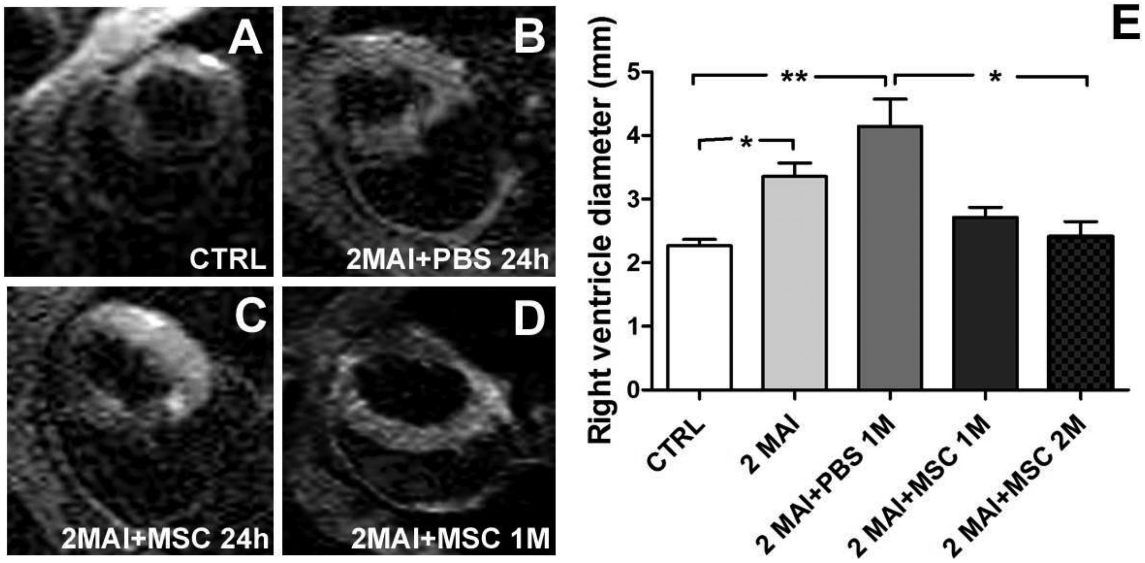

Figure 1. Heart morphology analyzed by MRI

Control and chagasic mice treated 2 months post- infection with PBS or MSC were analyzed by MRI to determine heart morphology and the presence of Feridex-labeled MSC . **(A-B)** Representative MRI showing a transversal image of the hearts in **(A)** CTRL. **(B)** 2MAI +PBS 24h. **(C)** 2MAI+MSC 24h. **(D)** 2MAI+MSC 1M groups. Labeled MSC are not detected in the heart tissue. **(E)** Graph showing the diameter of the right ventricle in different experimental groups. In this graph the animals from the groups 2MAI+PBS 24h and 2MAI+MSC 24h were combined in the group 2MAI. Improvement in RV diameter was observed at 1 month after treatment and was significant at 2 months. Group abbreviations: **CTRL**-control mice; **2MAI**-2 months after infection; **+PBS 24h** or **1M**-plus 24 hours or 1 month after PBS treatment, respectively; **+MSC 24h** or **1M** or **2M**-plus 24 hours or 1 or 2 months after MSC therapy, respectively. *P<0.05 and **P<0.01.

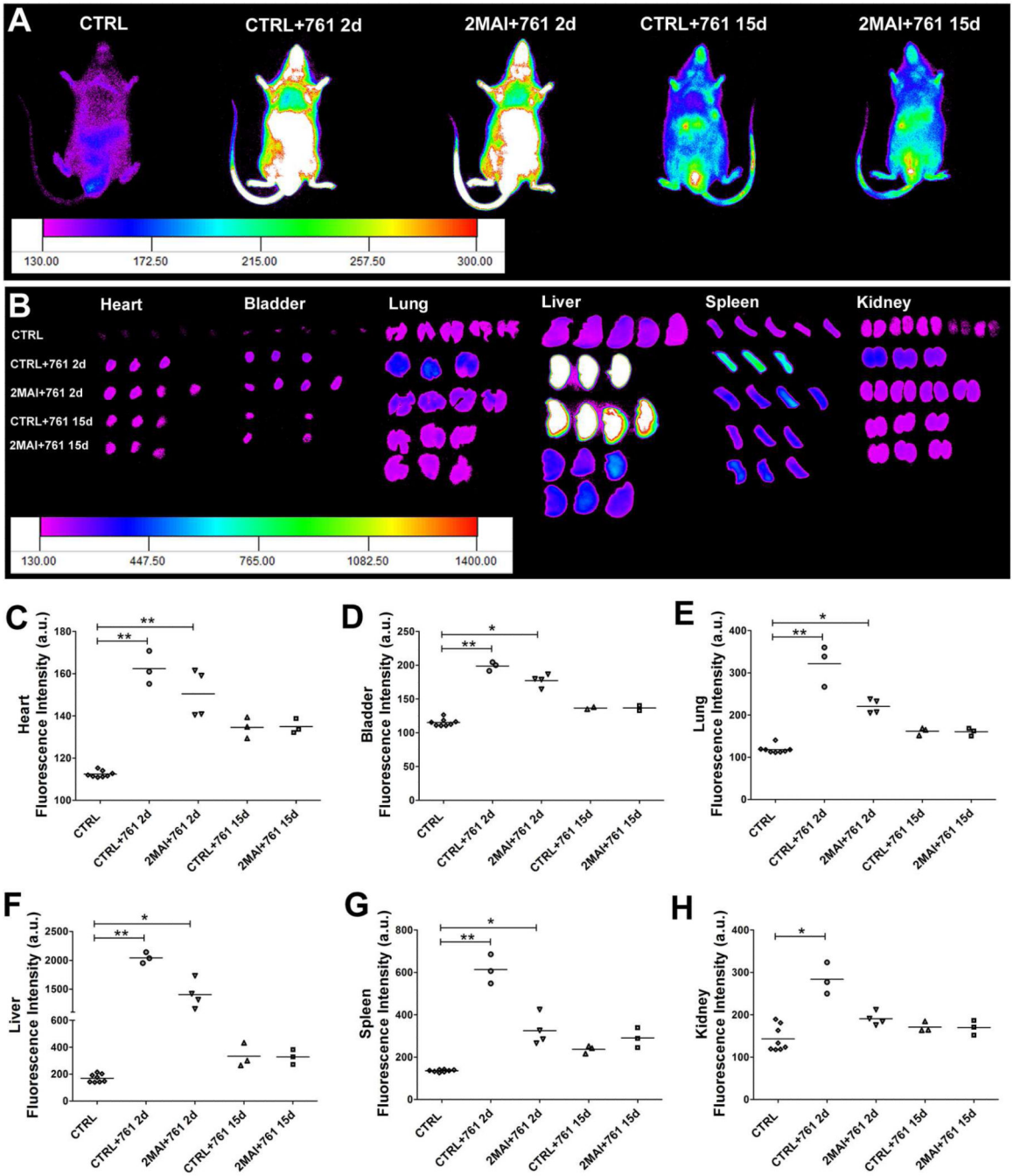

Figure 2. Distribution of free X-Sight761 nanoparticles

A PBS solution containing only nanoparticles was injected in the tail vein and tracked 2 or 15 days after injection by IVIS to determine the pattern of free nanoparticle distribution in control and chagasic mice. **(A)** Representative images showing the distribution of X-Sight761 viewed from the ventral surface of the body. **(B)** Images of ex vivo organs showing the nanoparticle distribution. **(C-H)** Quantification of fluorescence intensity of ex vivo organs shown in images in B. The evaluated organs were (**C**) heart, (**D**) bladder, (**E**) lung, (**F**) liver, (**G**) spleen and (**H**) kidney. Group abbreviations: **CTRL**-control mice;

2MAI-2 months after infection; **+761 2d** or **15d**-plus free X-Sight 761 nanoparticles after 2 or 15 days of the administration, respectively. *P<0.05 and **P<0.01.

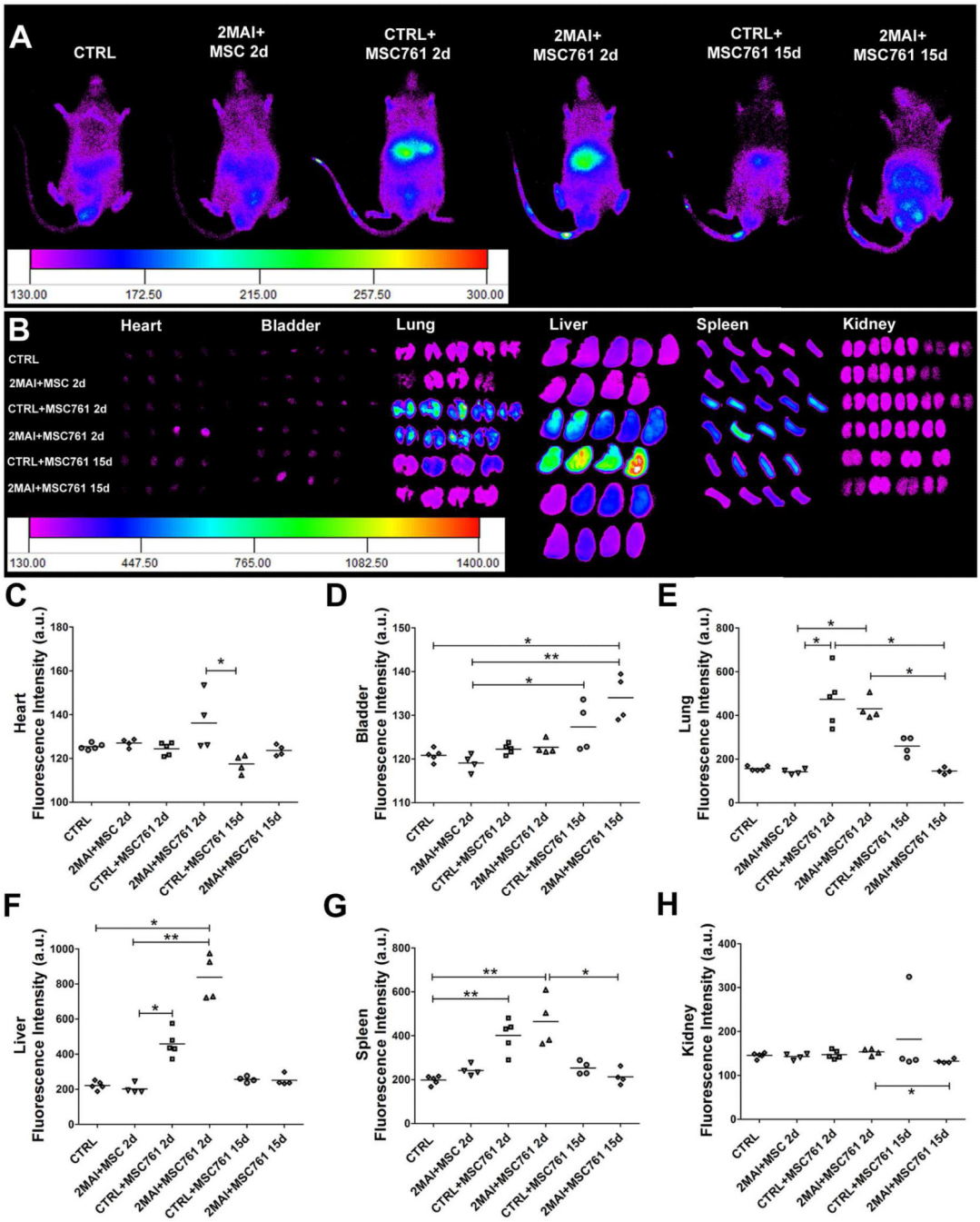

Figure 3. Tracking of X-Sight-labeled MSCs at 2 or 15 days after cell transplantation

The cells were intravenously injected in control and chagasic animals 2 months after infection and then tracked by IVIS 2 or 15 days after cell injection. (**A**) Representative images showing the distribution of transplanted MSCs viewed from the ventral surface of the body. (**B**) Images of ex vivo organs showing the distribution of labeled MSCs. **(C-H)** Quantification of fluorescence intensity of ex vivo organs shown in images in **B**. The evaluated organs were (**C**) heart, (**D**) bladder, (**E**) lung, (**F**) liver, (**G**) spleen and (**H**) kidney. Group abbreviations: **CTRL**-control mice; **2MAI**-2 months after infection; **+MSC761 2d** or

15d-plus X-Sight 761-labeled MSC after 2 or 15 days of the transplantation, respectively. *P<0.05 and **P<0.01.

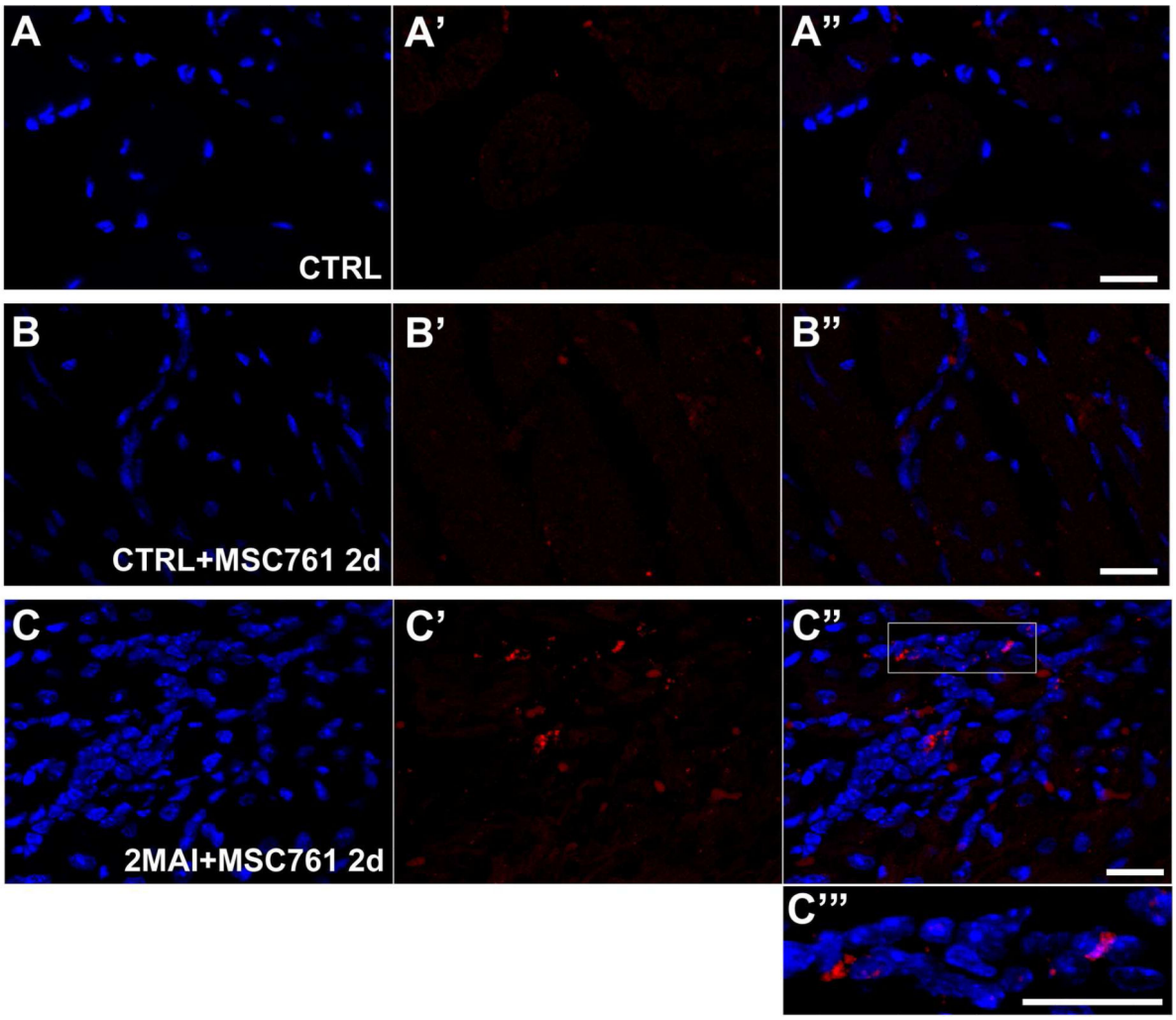

Figure 4. X-Sight-labeled MSCs tracking in the hearts by confocal microscopy

Hearts of control or chagasic mice treated with labeled MSC were sliced for confocal analysis (**A-C'"**) Representative confocal images showing X-Sight-labeled cells (red) in heart slices 2 days after therapy. (**A-A"**) CTRL. (**B-B"**) CTRL+MSC761 2d. (**C-C"**) 2MAI +MSC761 2d: (**A, B** and **C**) DAPI, (**A', B' and C**') X-Sight nanoparticles, and (**A", B" and C"**) Merged images. **(C"')** Two times magnified image of the white square on (C"). It is possible to note a higher concentration of MSCs in C, which is likely due to extravasation of inflammatory cells or attraction of other cells in the infected heart treated with MSC. Groups abbreviations: **CTRL**-control mice; **2MAI**-2 months after infection; **+MSC761 2d**-plus X-Sight 761-labeled MSC after 2 days of the transplantation, respectively. Scale bar = 20 μm.

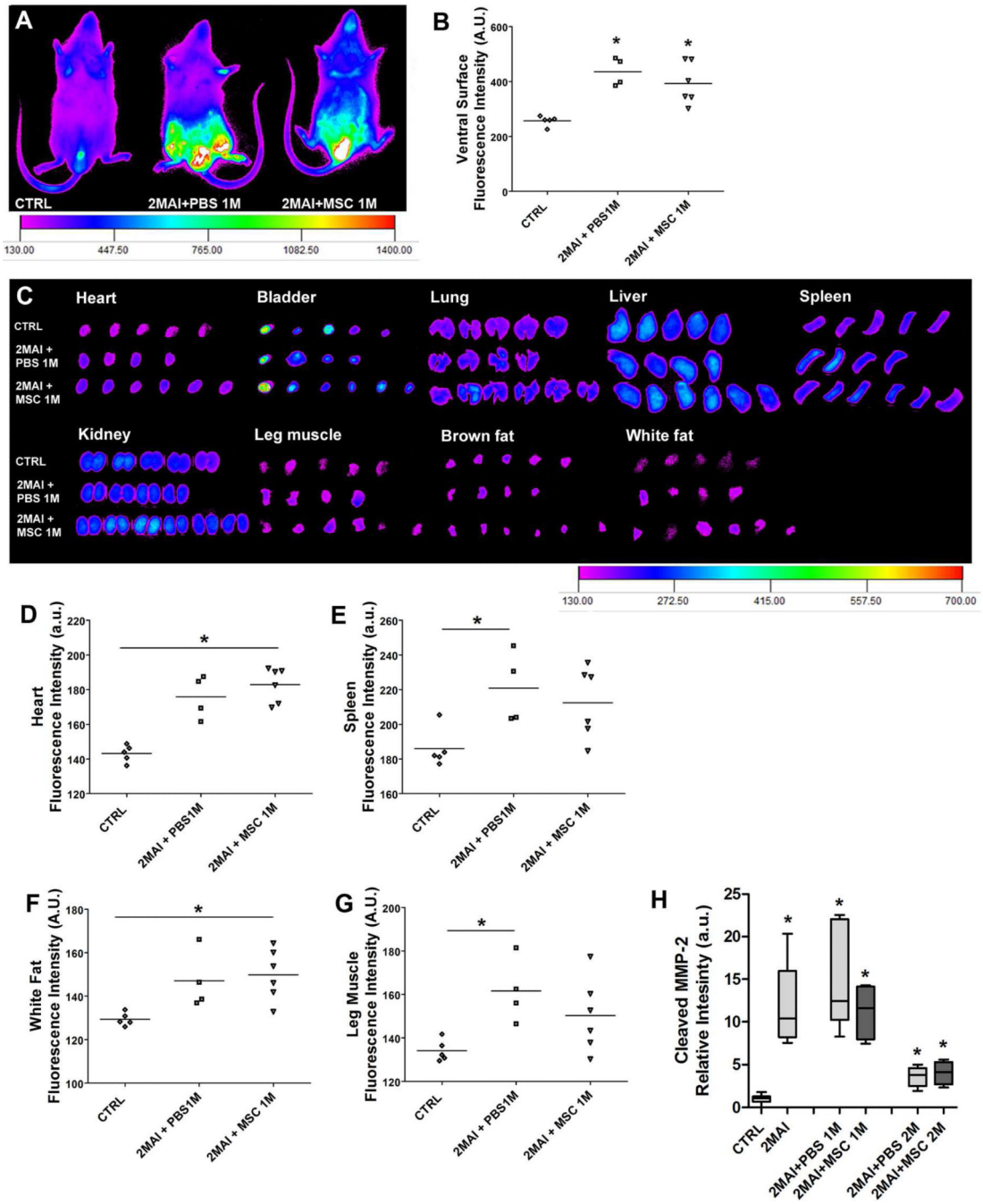

Figure 5. Quantification of global MMP activity

The mice received a tail vein injection of MMPSense750 48 hours before the imaging to detect MMP activity. Whole body and organ images from control and chagasic mice treated or not with MSCs were obtained by IVIS 1 month after PBS or cell treatment. **(A)** Representative images showing the distribution of MMPSense750 viewed from in the ventral surface of the body. **(B)** Quantification of whole body fluorescence intensity. **(C)** Representative images showing MMP activity in selected ex vivo organs. **(D-G)** Quantification of fluorescence intensity of ex vivo organs. The analyzed organs were heart,

bladder, lung, liver, spleen, kidney, leg muscle, brown fat and white fat. However only the graphs that present significant statistical differences are shown, which were **(D)** heart, **(E)** spleen, **(F)** white fat and **(G)** leg muscle. **(H)** Western blot of heart sample for cleaved MMP-2 protein. Group abbreviations: **CTRL**-control mice; **2MAI**-2 months after infection; **+PBS 1M** or **2M**-plus 1 or 2 months after PBS treatment; **+MSC 1M** or **2M-**plus 1 or 2 months after MSC therapy.

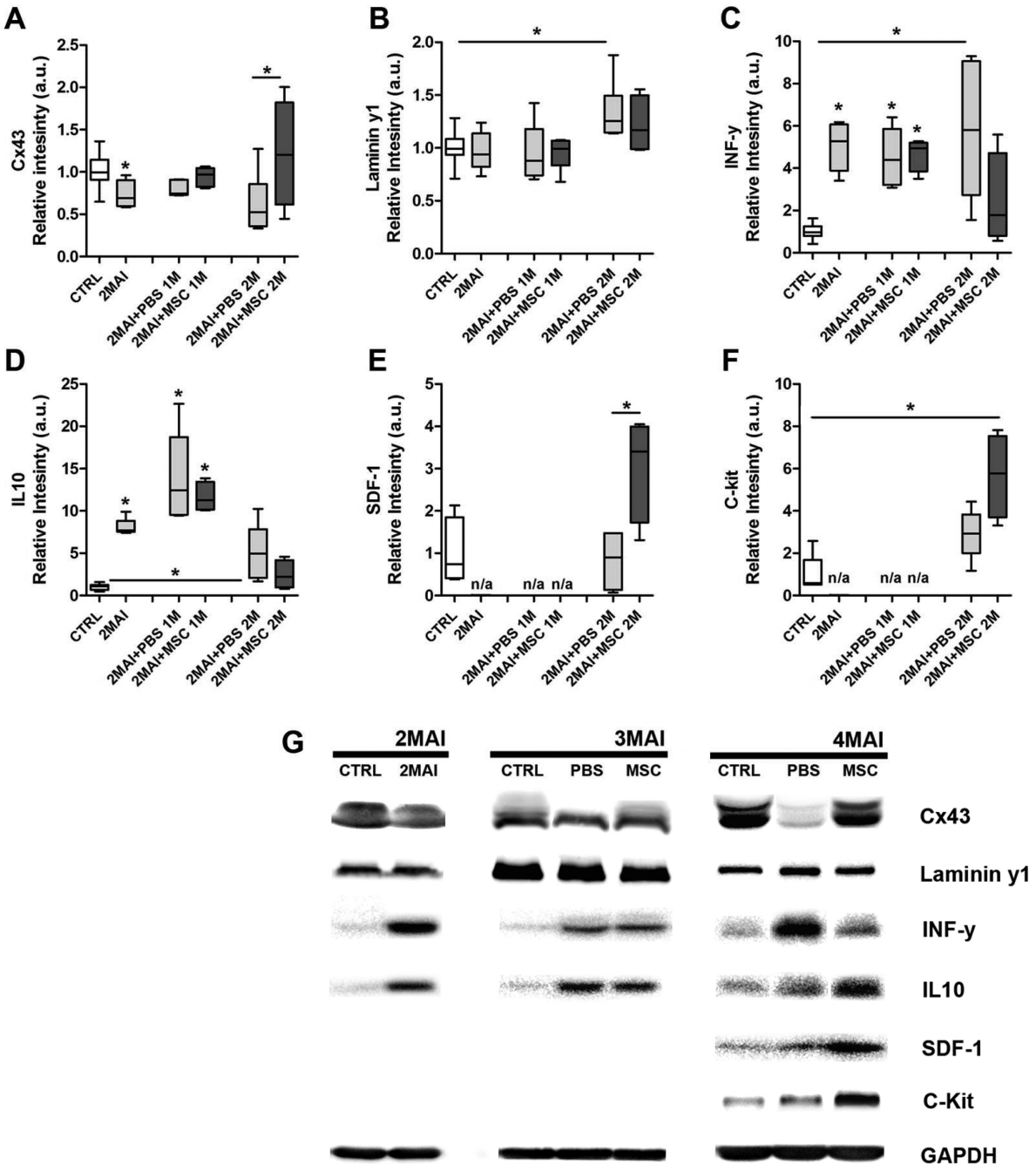

Figure 6. Western blot analysis of selected proteins in the heart of *T. cruzi* infected mice

The evaluated proteins included IL-10; IL-1β; INF-γ; Cx43; Cx37; occludin; laminin γ-1; ET-1; SDF-1; Stat-1; c-Kit; iNOS; cTnT; dystrophin and caveolin 3 but only the graphs which present statistical differences after MSC therapy are shown, including **(A)** Cx43 (although total Cx43 is shown, similar changes were observed in the phospho- and dephosphorylated isoforms, not illustrated), **(B)** laminin γ1, **(C)** INF-γ, **(D)** IL-10, **(E)** SDF-1 and **(F)** c-kit. **(G)** Representative images of the western blot assays. Each analyzed protein was statistically compared with its respectively control but protein levels were not compared among each other. Group abbreviations: **CTRL**-control mice; **2MAI**-2 months

after infection; **+PBS 1M** or **2M**-plus 1 or 2 months after PBS treatment; **+MSC 1M** or **2M-**plus 1 or 2 months after MSC therapy.